

**Universitat de Lleida**

Document downloaded from:

<http://hdl.handle.net/10459.1/59504>

The final publication is available at:

<https://doi.org/10.1109/TMECH.2017.2663436>

Copyright

(c) Institute of Electrical and Electronics Engineers (IEEE), 2017

# Kinect v2 Sensor-based Mobile Terrestrial Laser Scanner for Agricultural Outdoor Applications

Joan R. Rosell-Polo, Eduard Gregorio, Jordi Gené, Jordi Llorens, Xavier Torrent, Jaume Arnó,  
Alexandre Escolà

**Abstract**—Mobile terrestrial laser scanners (MTLS), based on light detection and ranging (LiDAR) sensors, are used worldwide in agricultural applications. MTLS are applied to characterize the geometry and the structure of plants and crops for technical and scientific purposes. Although MTLS exhibit outstanding performance, their high cost is still a drawback for most agricultural applications. This paper presents a low-cost alternative to MTLS based on the combination of a Kinect v2 depth sensor and a Real Time Kinematic (RTK) global navigation satellite system (GNSS) with extended color information capability. The theoretical foundations of this system are exposed along with some experimental results illustrating their performance and limitations. This work is focused on open-field agricultural applications, although most conclusions can also be extrapolated to similar outdoor uses. The developed Kinect-based MTLS (K2-MTLS) system allows to select different acquisition frequencies and fields of view (FOV), from one to 512 vertical slices. The authors conclude that the better performance is obtained when a FOV of a single slice is used, but at the price of a very low measuring speed. With that particular configuration, plants, crops, and objects are reproduced accurately. Future efforts will be directed to increase the scanning efficiency by improving both the hardware and software components and to make it feasible using both partial and full FOV.

**Index Terms**—Depth cameras, Kinect v2, LiDAR, RGB-D cameras, mobile terrestrial laser scanner (MTLS), precision agriculture, precision fructiculture, precision horticulture.

## I. INTRODUCTION

In the field of agriculture, LiDAR sensors are being profusely used in terrestrial measurement applications to map areas or objects of interest, both for

technical/commercial and scientific purposes [1]-[3]. Two configurations are commonly found in ground-based LiDAR measurement applications: terrestrial laser scanners (TLS) and mobile terrestrial laser scanners (MTLS). The former consists of a LiDAR with three degrees of freedom (3D LiDAR) mounted on a tripod [4]-[5]. Such systems can take measurements of the 3D features of the target scene from one single position (station). The result of the measurement is a 3D point cloud, consisting of the x, y, and z coordinates of each measured point referenced to the LiDAR location. By taking different measurements corresponding to several TLS stations and merging the corresponding point clouds, it is possible to build the resulting point cloud of large and complex scenes and objects (e.g., vegetation structure, and terrain characterization). MTLS consist of moving LiDAR-based systems designed to measure points of the intercepted objects in one plane at a time (2D LiDAR). The 3D point cloud is built by moving the LiDAR along the third dimension [6]-[8]. Therefore, in MTLS, the displacement of the LiDAR is necessary in order to obtain 3D point clouds. This is the opposite of TLS, wherein displacement is just an option. For more demanding applications, 3D LiDAR sensors are also used in MTLS configurations [9]. Although TLS and MTLS exhibit outstanding performance, their high cost is still a drawback for most agricultural applications.

The Microsoft Kinect sensor (hereafter Kinect) is probably the most popular and representative model of the recently developed low-cost color-depth (RGB-D) cameras, and for this reason, it is being widely used in a broad range of technological and scientific applications by R&D actors [10]-[13]. Designed to be used as a home video game complement, Microsoft's Kinect was thought to be used in indoor environments and particularly with low illuminance levels. This is why most technological developments and research works focus on the use of Kinect in indoor applications [14], [15]. Robotics is one research area where RGB-D sensors, and specifically Kinect, have been more intensively introduced for sensing and mapping, competing directly with other well-consolidated sensors like LiDAR-based (light detection and ranging) systems [16], [17].

This work was supported in part by the Spanish Ministry of Economy and Competitiveness under Grant AGL2013-48297-C2-2-R. Secretaria d'Universitats i Recerca from Departament d'Economia i Coneixement of the Generalitat de Catalunya is thanked for Mr. J. Gené's pre-doctoral fellowship (2016FI\_B 00669). Universitat de Lleida is also thanked for Mr. X. Torrent pre-doctoral fellowship.

Authors are with the Department of Agricultural and Forest Engineering, Research Group in AgroICT and Precision Agriculture, University of Lleida-Agrotecnio Center, Rovira Roure, 191, 25198 Lleida, Spain. Phone: +34 973 702861, fax: +34 973 702673 (e-mail: [jr.rosell@eagrof.udl.cat](mailto:jr.rosell@eagrof.udl.cat) (corresponding author); [egregorio@eagrof.udl.cat](mailto:egregorio@eagrof.udl.cat); [j.gene@eagrof.udl.cat](mailto:j.gene@eagrof.udl.cat); [jordi.llorens@eagrof.udl.cat](mailto:jordi.llorens@eagrof.udl.cat); [xavier.torrent@eagrof.udl.cat](mailto:xavier.torrent@eagrof.udl.cat); [JAarno@eagrof.udl.cat](mailto:JAarno@eagrof.udl.cat); [aescola@eagrof.udl.cat](mailto:aescola@eagrof.udl.cat)).

Commercially available low-cost RGB-D sensors (hereinafter, we will refer only to the Kinect sensor) can be an interesting alternative to LiDAR-based MTLs since high accuracy may not be critical in certain applications [18]-[20]. Moreover, these sensors can provide additional information, such as color and infrared, for each point of the cloud [13], [21], [22]. Kinect measurements in static mode, i.e., without movement, are similar to those undertaken by a stationary video camera, but the Kinect also provides distance data, allowing 3D point clouds to be obtained. Thus, in this common operational mode, the Kinect sensor performs similarly to a stationary TLS, although with a shorter range and a narrower field of view.

The Kinect sensor could also be a cost-effective alternative to MTLs. In this sense, most of such systems developed up to the present are based on the use of simultaneous localization and mapping (SLAM) techniques extensively used in robotic mapping [23], [24]. This paper presents a low-cost alternative approach to Mobile Terrestrial Laser Scanners (MTLS) with extended color information capability, based on the combination of Kinect v2 sensors (K2-MTLs) and a Real Time Kinematic (RTK) global navigation satellite system (GNSS). Within the framework of precision agriculture, this work focuses on the implementation and characterization of the Kinect in outdoor agricultural applications. The aim is to provide farmers with additional information about their crops to help them make better decisions. Most conclusions can also be extrapolated to similar outdoor uses other than in agriculture. This paper is structured as follows. First, some requirements of the sensing system are exposed. Next, the theoretical foundations are explained. Then, a brief compilation and comments on the Kinect v2 sensor and the RTK-GNSS characteristics are presented, continuing the exposition and discussion of the conducted experimental trials to assess the performance of the developed system. The paper ends with a compilation of the main conclusions of this work.

## II. THEORETICAL BASIS OF A KINECT V2-BASED MTLs

### A. Requirements of the Sensing System

The proposed K2-MTLs has to be suitable for general-purpose outdoor applications and particularly for agriculture/horticulture. This implies that availability of global navigation satellite systems (GNSS) is a premise and is the basis to geographically locate each measured point, thereby registering the captured point clouds at different time instants. That has to be achieved regardless the measuring field of view (FOV) of the developed system. The FOV is user-selectable, ranging from the full FOV ( $70^\circ \times 60^\circ$ ,  $512 \times 424$  measured points) to one vertical pixel column (424 measured points in a column or vertical plane).

### B. Theoretical development

The theoretical foundations of the developed system are explained. The goal is to determine the UTM coordinates of each point measured with the K2-MTLs system. To this end,

the configuration represented in Fig. 1 is considered. As it is shown, the K2-MTLs consists of a mobile RTK-GNSS antenna and two Kinect v2 sensors, designated as K#1 and K#2. In the illustration, K#1 is measuring point  $P_1$  on the left tree, while K#2 is measuring point  $P_2$  on the right tree, both relative to the forward direction (path of the K2-MTLs). Although each Kinect sensor is able to simultaneously measure the distance of  $512 \times 424$  points, it has been chosen to represent only the points  $P_1$  and  $P_2$  for the sake of simplicity. The following development only considers the point  $P_1$ , whereas the coordinates of  $P_2$  and of any other point can be obtained in a similar way.

The position of the GNSS antenna in UTM coordinates is given by  $\mathbf{r}_{GNSS} = [x_{GNSS}, y_{GNSS}, z_{GNSS}]$ , whereas the position of K#1 relative to the antenna is represented by  $\mathbf{r}_{K1} = [x_{K1}, y_{K1}, z_{K1}]$ . In the configuration shown in Fig. 1, both the antenna and the sensors are attached to the same structure and therefore the vector  $\mathbf{r}_{K1}$  is time-invariant.

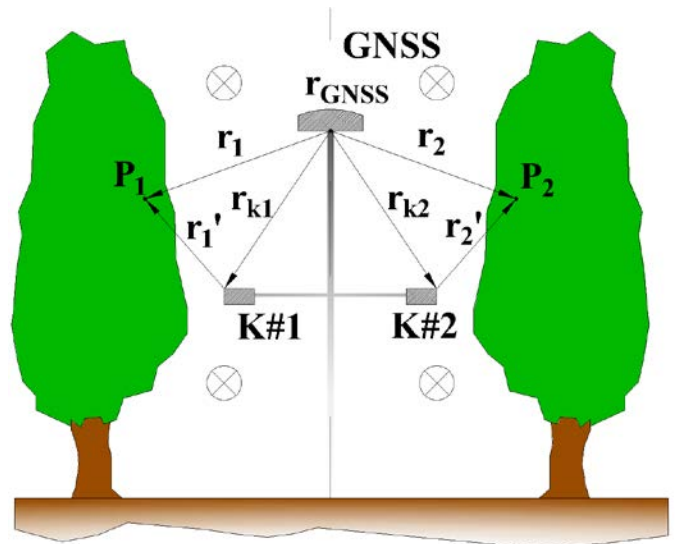


Fig. 1. Typical configuration of the K2-MTLs with two Kinect sensors (K#1 and K#2) and a RTK-GNSS antenna. Points on trees on both sides ( $P_1$  and  $P_2$ ) are simultaneously measured. The forward direction of the K2-MTLs is pointing toward the paper ( $\otimes$ ).

On the other hand, the position of  $P_1$  relative to the antenna is given by  $\mathbf{r}_1 = [x_1, y_1, z_1]$ , whereas its position relative to K#1 is  $\mathbf{r}'_1 = [x'_1, y'_1, z'_1]$ , calculated as

$$\mathbf{r}_1 = \mathbf{r}_{K1} + \mathbf{r}'_1 = [x_{K1} + x'_1, y_{K1} + y'_1, z_{K1} + z'_1]. \quad (1)$$

The UTM coordinates of  $P_1$  can be calculated as

$$\begin{aligned} \mathbf{R}_{P1} &= [x_{UTM_{P1}}, y_{UTM_{P1}}, z_{UTM_{P1}}] \\ \mathbf{R}_{P1} &= \mathbf{r}_{GNSS} + \mathbf{r}_1 = \mathbf{r}_{GNSS} + \mathbf{r}_{K1} + \mathbf{r}'_1 = \\ &= [x_{GNSS} + x_{K1} + x'_1, y_{GNSS} + y_{K1} + y'_1, z_{GNSS} + z_{K1} + z'_1]. \end{aligned} \quad (2)$$

Fig. 2 shows the projection of the K2-MTLs on the  $X_{UTM}$ - $Y_{UTM}$  plane, where  $X_{UTM}$  is the East-West axis, and  $Y_{UTM}$  is the North-South axis. Furthermore,  $X'$ - $Y'$  is the coordinate system of K#1 (horizontal plane of the sensor), where  $X'$  is the axis

parallel to the path of the K2-MTLS but in the opposite direction, and  $Y'$  is the axis corresponding to depth measurements<sup>1</sup>. It is assumed that the horizontal plane of the sensor ( $X'$ - $Y'$ ) is parallel to the ground ( $X_{UTM}$ - $Y_{UTM}$ ).

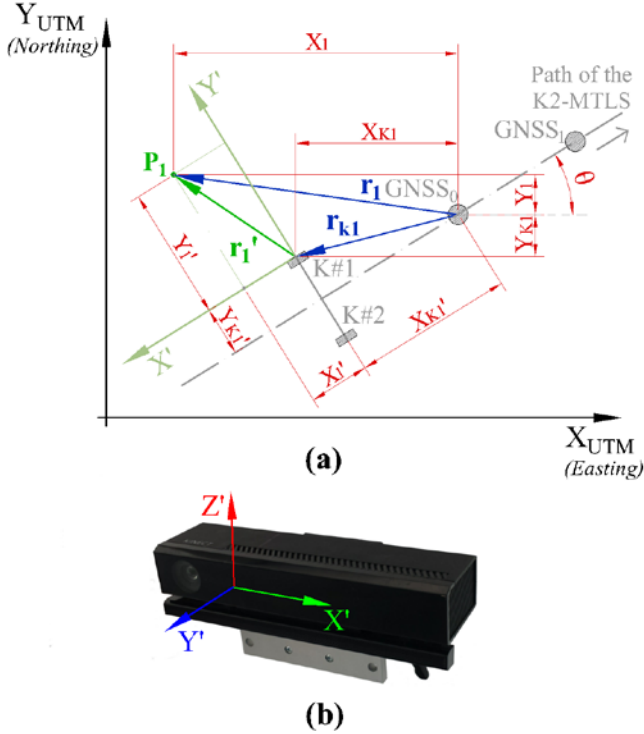


Fig. 2. Coordinate systems and vectors on which the theoretical development is based. (a) Top view of the K2-MTLS. (b) Kinect axes designation.

Vectors  $r_1$ ,  $r_{k1}$  and  $r_i$  have been previously presented, while the angle  $\theta$  represents the direction of motion (path) of the K2-MTLS relative to  $X_{UTM}$ . This angle can be computed from the position of the RTK-GNSS antenna in two different time instants,  $GNSS_0 = [x_{GNSS0}, y_{GNSS0}]$  and  $GNSS_1 = [x_{GNSS1}, y_{GNSS1}]$ , resulting in

$$\cos\theta = \frac{(x_{GNSS1} - x_{GNSS0})}{\sqrt{(x_{GNSS1} - x_{GNSS0})^2 + (y_{GNSS1} - y_{GNSS0})^2}} \quad (3)$$

$$\sin\theta = \frac{(y_{GNSS1} - y_{GNSS0})}{\sqrt{(x_{GNSS1} - x_{GNSS0})^2 + (y_{GNSS1} - y_{GNSS0})^2}} \quad (4)$$

Components of  $r_1$  on the horizontal plane are deduced by applying trigonometric relationships:

$$x_1 = x'_1 \cos\theta + y'_1 \sin\theta + x_{K1} \quad (5)$$

$$y_1 = y'_1 \cos\theta - x'_1 \sin\theta - y_{K1} \quad (6)$$

In the previous expressions,  $x_{K1}$  and  $y_{K1}$  are unknown. In practice, the position of K#1 relative to the antenna is measured on the coordinate system  $X'$ - $Y'$  (parallel and perpendicular to the path of the MTLs), obtaining  $x'_{K1}$  and  $y'_{K1}$ . From Fig. 2 it follows:

$$x_{K1} = x'_{K1} \cos\theta + y'_{K1} \sin\theta \quad (7)$$

$$y_{K1} = x'_{K1} \sin\theta - y'_{K1} \cos\theta \quad (8)$$

The vertical component (height) of  $r_1$  is given by

$$z_1 = z'_1 - z_{K1} \quad (9)$$

From (2), (5), (6) and (9), the UTM coordinates of  $P_1$  can be expressed as

$$x_{UTM_{P1}} = x_{GNSS} - x_1 \quad (10)$$

$$y_{UTM_{P1}} = y_{GNSS} + y_1 \quad (11)$$

$$z_{UTM_{P1}} = z_{GNSS} + z_1 \quad (12)$$

### III. EXPERIMENTAL ASSESSMENT

This section includes the description of the K2-MTLS components as well as the field trials conducted to test the system performance. It exposes and discusses the most significant results obtained.

#### A. Characteristics of the K2-MTLS components

A Microsoft Kinect v2 and a Leica GNSS1200 RTK connected to a laptop computer via two respective USB ports are the main hardware components of the developed K2-MTLS system. These components are mounted on an autonomous hybrid vehicle whose speed can be adjusted by the user over a wide range (Fig. 3). Specifically developed software synchronously acquires both the Kinect and GNSS raw data and saves them into a file. The software allows the user to select different FOV and acquisition frequencies and shows the RGB and IR video frames of the measured scenes viewed by the K2-MTLS in real time.

TABLE I  
CHARACTERISTICS OF THE K2-MTLS SYSTEM

Principle of operation		Time of flight
Working range (m)	Minimum: 0.5	Maximum (depends on measuring conditions) 4.5--8
Maximum measuring frequency (Hz)	~ 5-10	Depends on the measurement configuration and computer performance
FOV of IR and Depth channel (columns/degrees)	Vertical Horizontal	424 / 60° Min. 1; Max. 512 / 70°
RGB channel	Resolution (pixels) FOV	1920 x 1080 84.1° x 53.8°
RTK-GNSS acquisition frequency (Hz)		20
RTK-GNSS accuracy (cm)		< 2

<sup>1</sup> In the original coordinate system of the Kinect, the Z axis indicates depth, and the Y axis indicates height. In this paper, the Z and Y axes are designated

$Y'$  and  $Z'$ , respectively. This simplifies the theoretical development since  $Z'$  is parallel to  $Z_{UTM}$ .

Subsequently, a second program, based on the theoretical basis explained in section II, transforms raw data files into UTM georeferenced 3D point clouds with x, y, z, RGB, and infrared (IR) information for each point of the scanned object. Due to the known limitation of Kinect sensors, outdoor illuminance levels must be kept low enough to allow high quality measurements [13], making nocturne artificially lighted measurements an alternative option. Table I summarizes the main characteristics of the developed K2-MTLs system.

### B. Experimental Setup

Experimental data were obtained during the summer season of 2016 at the campus of the School of Agrifood and Forestry Science and Engineering (ETSEA) of the University of Lleida (UdL) (41°37'45"N 0°35'47"E, altitude 188 m a.s.l.). Two different scenarios were chosen to test the performance of the system. The first scenario was an outdoor concrete area with a widely used machinery combination (tractor-sprayer) as an object to be scanned, while the second scenario was a row of vines.

The platform used to move the sensing system was the mobile platform designed by the GRAP-UdL research group, shown in Fig. 3. A vertical mast was firmly fixed to the mobile structure to which all the electronic elements were attached. The RTK-GNSS antenna was located on the top position at a height of 2 m. In this experimental trial, only one Kinect sensor was used, corresponding to K#1 in Fig. 1 and Fig. 2. Additionally, an artificial source of light was installed to improve lighting conditions for some of the scanning tests. The vehicle carried a laptop computer to control and acquire data from the sensors.



Fig. 3. Mobile platform and sensing system including the Kinect v2 sensor and the RTK-GNSS receiver.

The platform was able to successfully and smoothly drive forward and backward along a marked path thanks to two rubber tracks moved by electrical AC motors. The forward speed can be accurately adjusted by changing the AC power frequency. Fig. 4 shows the platform working in both scanning scenarios.

The operational parameters of the different tests can be found in Table II. For each scenario, three FOV configurations were tested. Full FOV is characterized by the acquisition of complete frames covering a width of 512 pixels columns each.



Fig. 4. (a) K2-MTLs outdoor scanning application (Scenario 1). (b) K2-MTLs agricultural scanning application (Scenario 2).

Thus, continuous scanning of an object with accurate juxtaposition of frames can only be performed if an adequate frame rate (or sampling frequency) and synchronized forward speed are set. Adopting a partial FOV (100 pixels columns) reduces the field of view (Table II), and if the forward speed remains the same, makes a higher frame rate necessary in order to obtain a continuous scanning of objects or vegetation. The extreme case is to limit the field of view to a single pixel column (single FOV) every time the Kinect emits and captures a frame. Given a certain sensor-target distance, each FOV configuration needs a particular frame rate to be adjusted to achieve the juxtaposition of frames. At the same time, the capture settings of the Kinect must be synchronized with the forward speed of the mobile platform that will also be variable depending on the FOV adopted.

TABLE II  
OPERATIONAL PARAMETERS DURING FIELD TESTS

	Single-column FOV	Narrow FOV	Full FOV
<b>Scanning in outdoor applications (Scenario 1)</b>			
FOV (columns)	1 (255)	100 (205 to 304)	512 (1 to 512)
Frame interval (ms)	194	4150/3320/2490	17000
Frame rate (Hz)	5.15	0.24/0.30/0.40	0.06
Speed (m/s)	0.043	0.256	0.256
<b>Scanning in agricultural applications (Scenario 2)</b>			
FOV(columns)	1 (255)	100 (205 to 304)	512 (1 to 512)
Frame interval (ms)	194	1660/1328/996	6800
Frame rate (Hz)	5.15	0.60/0.75/1.00	0.15
Speed (m/s)	0.043	0.256	0.256

### C. Results and Discussion

A point cloud was obtained for each scanning test, being possible to visualize the point cloud of the object in raw x, y, and z coordinates, and, if applicable, infrared (IR) or RGB values using CloudCompare software (EDF R&D Telecom ParisTech, 2014). All these data were imported and stored in an ASCII format. An example of these data is shown in Fig. 5, where a single-column FOV was used for an outdoor scanning

application (Scenario 1). Blue points at the bottom area of the RGB point cloud are points with  $x$ ,  $y$ , and  $z$  data but without RGB and IR information due to the different FOV of the RGB and IR/depth cameras of the Kinect sensor (Table I).

Regarding the accuracy of the data (Fig. 5), the point cloud seems to represent objects in a very reliable way when a single-column FOV is used. Fig. 5(a) shows the variation of the  $z$  coordinate. IR data in Fig. 5(b) show the returned signal intensity for each pixel. Finally, RGB faithfully reproduces the colors of the combination tractor-sprayer (Fig. 5(c)), allowing the different parts or basic elements to be identified. Therefore, this output information is finally taken as reference to evaluate the tests discussed in the following sections.

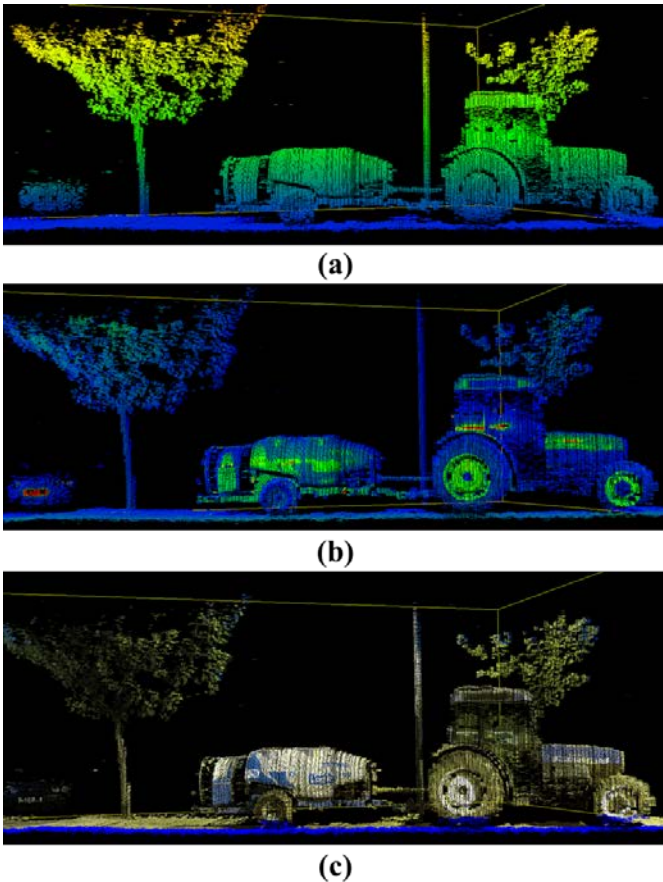


Fig. 5. K2-MTLs outdoor scanning application using a single-column FOV. (a) Point cloud with a height color ramp. (b) Point cloud with an infrared return intensity color ramp (red highest, blue lowest). (c) Point cloud with RGB color information.

### Scenario 1. K2-MTLs scanning in outdoor applications

Two analyses were performed in Scenario 1. In the first one (Fig. 6), different frame rates were adjusted for a partial FOV (100 slices). Depending on the frame rate, it was possible to accurately juxtapose frames (at 0.30 Hz) or, conversely, separate or overlap about 25% if 0.24 Hz or 0.40 Hz frame acquisition frequencies were used, respectively. According to the graphical results, significant differences were found when the frame rate was modified. For low frequencies (0.24 Hz), similar gaps were produced whether forward speed was kept

constant, such as shown in Fig. 6(a). Nevertheless, the object was not deformed excessively. In contrast, for high frequencies (0.40 Hz), an overlapping effect was evident (Fig. 6(c)), producing a clear deformation of the object. On the contrary, in the vertical axis this effect was not present. It is then recommended, with the specific measuring configuration used in this Scenario 1, using frequencies around 0.30 Hz to get a better representation.

Another issue, as seen in Fig. 6, is the erroneous assignments of color to points in both partial and full FOV measurements. In fact, a specific analysis would be required to identify the causes of the observed problems in Scenario 1. On the one hand, they may be due to the sensor operation. On the other hand, more likely, due to limitations of the developed software and processing computer as well as to the sensor mounting structure when capturing high amount of data as in the case of partial and full FOV.

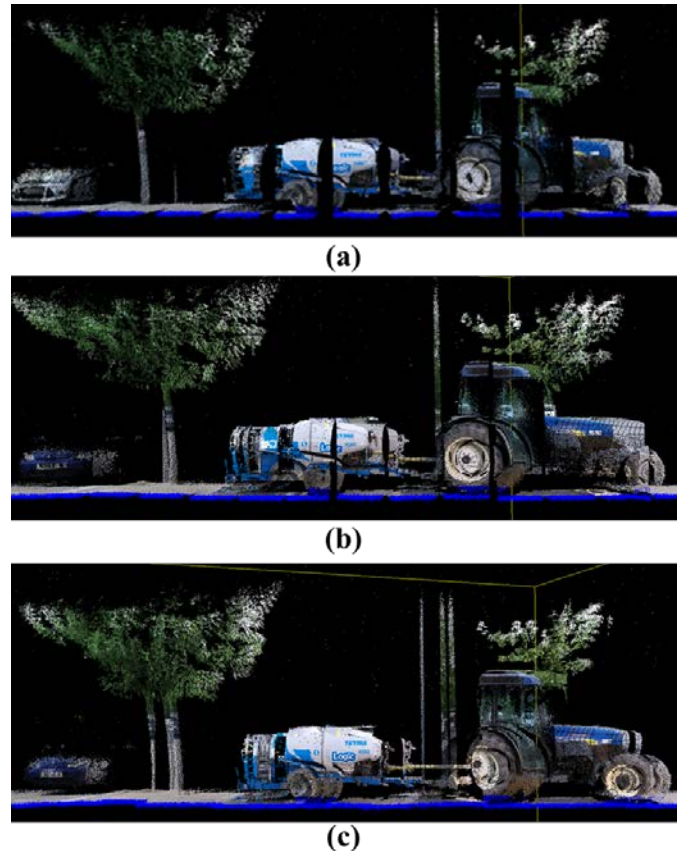


Fig. 6. Graphical representation of RGB point clouds of Scenario 1 obtained with a partial FOV of 100 columns per frame at different frame acquisition frequencies: (a) 0.24 Hz, (b) 0.30 Hz, and (c) 0.40 Hz.

The second analysis focused on comparing three RGB-point clouds corresponding to three different FOV (Fig. 7) that were configured to attempt to obtain a correct juxtaposition of frames. Specific analyzed FOV were single-column FOV (1 col), partial FOV (100 cols) and full FOV (512 cols). When the single-column FOV was used (Fig. 7(a)), an accurate shape of the scanning object was obtained. However, adjusting the Kinect requires a high frame acquisition frequency and a very low forward speed, causing low working efficiencies. By

increasing the FOV, the working efficiency was improved, but spatial synchronization problems appeared as a result of the generation of some gaps and overlaps. Only when accurate geometrical characterization is not required, it could be interesting to assess the possibility to choose a partial FOV (Fig. 7(b)) or full FOV (Fig. 7(c)) with the aim of increasing the scanning efficiency.

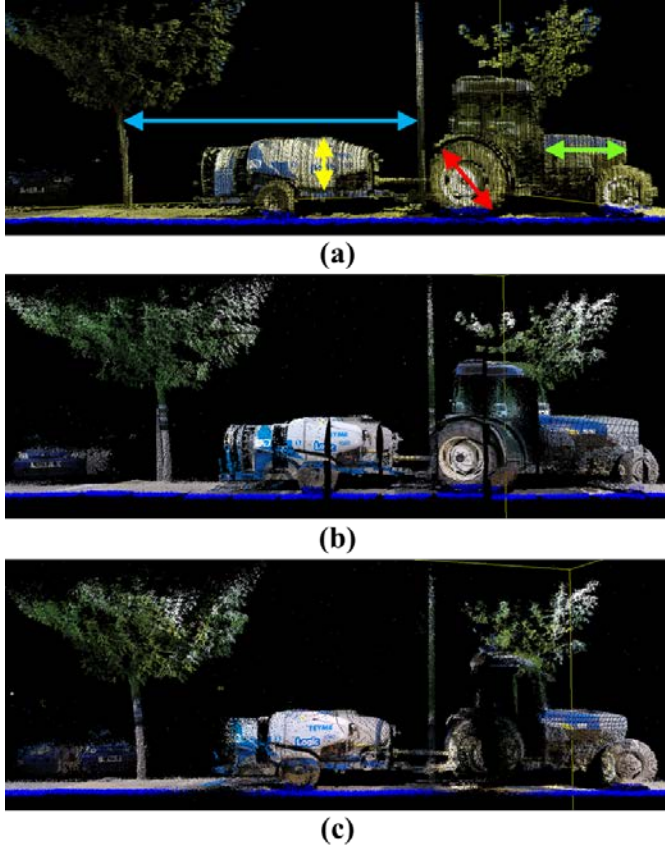


Fig. 7. Graphical representation of RGB point clouds in Scenario 1 obtained with different FOV. (a) Single-column FOV at 5.15 Hz. Colored arrows show the distances used for measurement comparison. (b) Partial FOV at 0.30 Hz. (c) Full FOV at 0.06 Hz.

A simple quantitative comparison between manually measured real distances and those extracted from the point cloud was made (Fig. 7). The obtained results, shown in Table III, reveal moderate distance errors, up to 11.6%. The reasons why the errors are so much greater for the partial FOV than for the full FOV are not evident as several causes could contribute, as previously said. The current version of the developed software and the performance of the computer specifically used in the test could lead to different real-time data processing performances and outputs which could be reflected in the obtained results. For example, the amount of data to be processed in the one single column FOV is much lower than in the case of partial and full FOV. This can result in better processing (hardware and software) performance in the single column case and in lower measurement errors. Comparing the partial and full FOV cases, although the latter implies processing much more data than the former, their frame rate is lower and, therefore, the hardware and software real performances are not necessarily the same. Furthermore, in the

full FOV case, fewer wider point clouds are merged than in the partial FOV case, what presumably can lead to more precise representation of the measured objects, as it was really obtained according to the corresponding measured errors.

TABLE III  
COMPARISON BETWEEN REAL AND MEASURED DISTANCES IN SCENARIO 1  
WITH A SINGLE-COLUMN FOV

	D1	D2	D3	D4
<b>Real distance (cm)</b>	570	90	138	132
<b>Single-col. FOV at 5.15 Hz</b>				
Measured distance (cm)	573	90	137	134
Error (%)	0.5	0	-0.7	1.5
<b>Partial FOV at 0.30 Hz</b>				
Measured distance (cm)	538	80	154	118
Error (%)	-5.6	-11.1	11.6	-10.6
<b>Full FOV at 0.06 Hz</b>				
Measured distance (cm)	565	85	132	117
Error (%)	-0.9	-5.6	-4.3	-11.4

D1: Tree-pole (blue); D2: Sprayer tank height (yellow); D3: Tractor hood length (green); D4: Rear wheel diameter (red).

### Scenario 2. K2-MTLs scanning in agricultural applications

To compare the results of different FOV in agricultural crops (Table II), the K2-MTLs was used on a row of vines using different configuration settings. Like in Scenario 1, there were significant differences depending on the configuration used. Fig. 8 shows the point cloud obtained with the K2-MTLs for the scanned vines using a single-column FOV configuration. As before, users can select three types of output data according to the desired application: x, y, and z point cloud (Fig. 8(a)), infrared return intensity point cloud (Fig. 8(b)), and RGB point cloud (Fig. 8(c)).

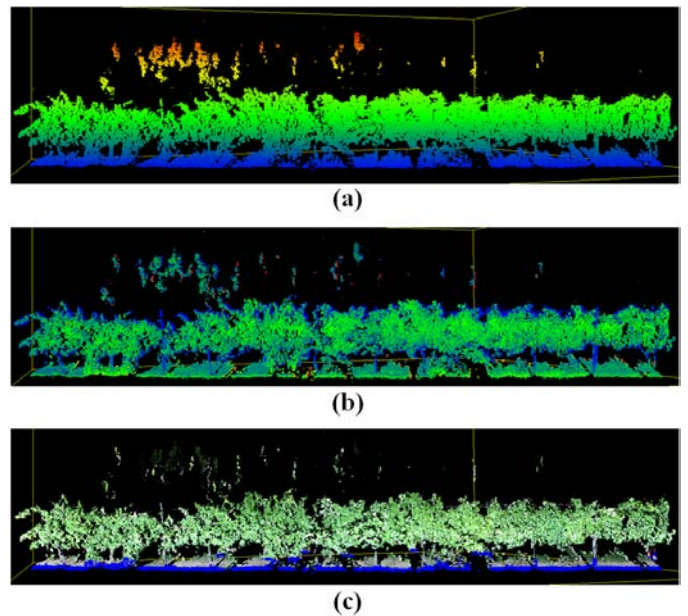


Fig. 8. K2-MTLs scanning application in vines using a single-column FOV. (a) Point cloud with a height color ramp. (b) Point cloud with an infrared return intensity color ramp. (c) Point cloud with RGB color information.

Fig. 9 shows the RGB point clouds obtained with different FOV. By simple visual comparison, the use of a single-column FOV (Fig. 9(a)) appears again more reliable because it reproduces the shape and the structural arrangement of the vines more clearly and accurately. On the other hand, some gaps are evident when wider FOV are used (Fig. 9(b) and (c)), even when both the frame rate and forward speed have been properly adjusted. In short, the lack of continuity in scanning the vegetation could be a limiting factor for the applicability of the system under field conditions. Conversely, reducing the FOV to a single column improves the performance of the system, but at the expense of a significant reduction in the working efficiency. It is also true that tree crops may have irregular canopy shapes and may be spatially variable, so a system that continuously scans the rows in a more reliable way is a better option.

Fig. 10 shows in greater detail the result of the operation of the K2-MTLs in vines. Using full FOV with correct juxtaposition (Fig. 10(b)) requires intermittent activation of the Kinect using low frame rates (0.15 Hz). Whenever activation occurs, the sensing system has moved 1.74 m along the row. This mode of operation causes the vision of vines from different angles, and a perpendicular view of the canopy only occurs in those positions along the row in which the Kinect is activated (every 1.74 m). This feature could justify the use of a single-column FOV when extracting information about the canopy despite the drawback of a slower operation.

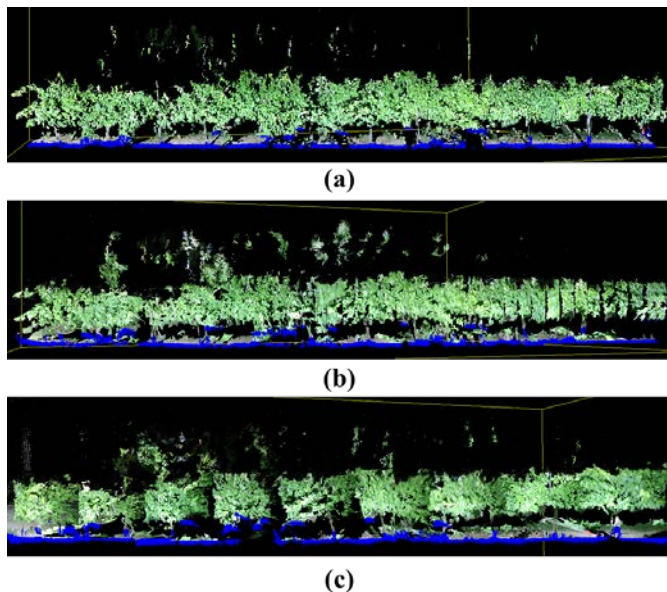


Fig. 9. Graphical representation of RGB point clouds in Scenario 2 obtained with different FOV: (a) Single-column FOV at 5.15 Hz, (b) partial FOV at 0.75 Hz, and (c) full FOV at 0.15 Hz.

Another application could be the use of the K2-MTLs at different sampling points within a plot. In this case, a wider FOV would be an option if the vegetative parameter of interest could be obtained from a single frame. Then, a comparison between a partial and full FOV is required in this case.

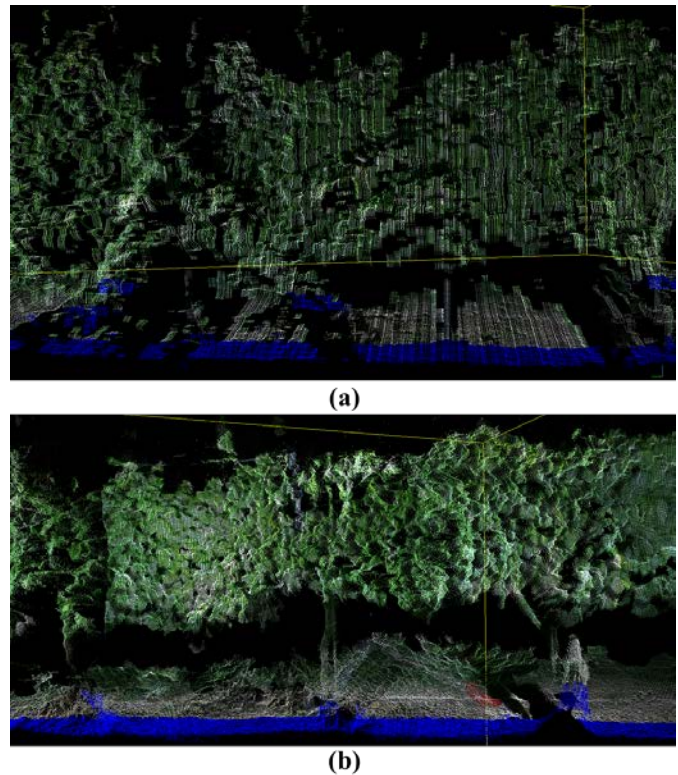


Fig. 10. Vineyard scanning detail. (a) Single-column FOV. (b) Full FOV.

#### IV. CONCLUSION

This work presents a low cost, yet effective, Mobile Terrestrial Laser Scanner for agricultural applications, based on a combination of a Kinect v2 sensor and a RTK-GNSS. The K2-MTLs can be used for scanning objects and crops. In combination with RTK-GNSS, point clouds are captured at different time instants and georeferenced for location. Better performance of the Kinect is obtained by adjusting the emission and capture of frames for a single slice (single FOV) since vegetation and geometric shapes are reproduced in a more accurate way (errors up to 1.5%). However, when accurate geometrical characterization is not required, a wider field of view (partial FOV) can be used to improve working efficiency. In order to increase the scanning efficiency with single-column FOV, future work will focus on stepping up the frame rate by improving both the acquisition software and the computer performance. In addition, hardware components like a gimbal and/or an inertial measurement unit (IMU) will be mounted to compensate the measuring errors due to vibrations and misalignments of the K2-MTLs as it moves along the field. This fact would allow improvement of the spatial synchronization of adjacent point clouds, making this feasible using both partial and full FOV.

## REFERENCES

- [1] J. Wei and M. Salyani, "Development of a laser scanner for measuring tree canopy characteristics: Phase I. Prototype development," *T. ASAE.*, vol. 47 no.6, pp. 2101-2107, Nov. 2004.
- [2] J.R. Rosell-Polo and R. Sanz, "A review of methods and applications of the geometric characterization of tree corps in agricultural activities," *Comput. Electron. Agr.*, vol. 81, pp. 124-141, Feb. 2012.
- [3] R. Sanz, J. Llorens, A. Escolà, J. Arnó, M. Ribes-Dasi, J. Masip, F. Camp, F. Gràcia, F. Solanelles, S. Planas, T. Pallejà, J. Palacín, E. Gregorio, I. del-Moral-Martínez and J.R. Rosell-Polo, "Innovative LIDAR 3D Dynamic Measurement System to Estimate Fruit-Tree Leaf Area," *Sensors* vol. 11, no.6, pp. 5769-5791, May. 2011.
- [4] K.E. Keightley and G.W. Bawden, "3D volumetric modelling of grapevine biomass using Tripod LiDAR," *Comput. Electron. Agr.*, vol. 74 no.2, pp. 305-312, Nov. 2010.
- [5] I. Moorthy, J.R. Miller, J.A.J. Berni, P. Zarco-Tejada, B. Hu, and J. Chen, "Field characterization of olive (*Olea europaea* L.) tree crown architecture using terrestrial laser scanning data," *Agr. Forest Meteorol.*, vol. 151, no. 2, pp. 204-214, Feb. 2011.
- [6] D. Andújar, A. Escolà, J.R. Rosell-Polo, C. Fernández-Quintanilla, J. Dorado, "Potential of a terrestrial LiDAR-based system to characterise weed vegetation in maize crops," *Comput. Electron. Agr.*, vol. 92, pp. 11-15, Mar. 2013.
- [7] J.R. Rosell-Polo, R. Sanz, J. Llorens, J. Arnó, A. Escolà, M. Ribes-Dasi, J. Masip, F. Camp, F. Gràcia, F. Solanelles, T. Pallejà, L. Val, S. Planas, E. Gil and J. Palacín, "A tractor-mounted scanning LIDAR for the non-destructive measurement of vegetative volume and Surface area of tree-row plantations: A comparison with conventional destructive measurements," *Biosyst. Eng.*, vol. 102, no. 2, pp. 128-134, Feb. 2009.
- [8] J.R. Rosell-Polo, J. Llorens, R. Sanz, J. Arnó, M. Ribes-Dasi, J. Masip, A. Escolà, F. Camp, F. Solanelles, F. Gràcia, E. Gil, L. Val, S. Planas, and J. Palacín, "Obtaining the three-dimensional structure of tree orchards from remote 2D terrestrial LIDAR scanning," *Agr. Forest Meteorol.*, vol. 149, pp. 1505-1515, Sep. 2009.
- [9] C. Glennie and D.D. Lichti, "Static calibration and analysis of the velodyne HDL-64E S2 for high accuracy mobile scanning," *Remote sensing*, vol. 2, pp. 1610-1624, Jun. 2010.
- [10] Z. Zhang, "Microsoft Kinect sensor and its effect," *IEEE Multimedia*, vol. 19 no. 2, art. 6190806, pp. 4-10, Feb. 2012.
- [11] Y.-J. Chang, S.-F. Chen, J.-D. Huang, "A Kinect-based system for physical rehabilitation: A pilot study for Young adults with motor disabilities," *Res. Dev. Disabil.*, vol. 32 no. 6, pp. 2566-2570, Nov. 2011.
- [12] M. Stommel, M. Beetz and W. Xu, "Model-free detection, encoding, retrieval, and visualization of human poses from Kinect data," *IEEE-ASME T. Mech.*, vol. 20 no.2, pp. 865-875, Ap. 2015.
- [13] J.R. Rosell-Polo, F. Auat Cheein, E. Gregorio, D. Andújar, L. Puigdomènech, J. Masip, and A. Escolà, "Advances in structured light sensors Applications in precision agriculture and livestock farming," *Adv. Agron.*, vol. 133, pp. 71-112, Sep. 2015.
- [14] K. Khoshelham, S.O. Elberink, "Accuracy and resolution of Kinect depth data for indoor mapping applications," *Sensors*, vol. 12 no. 2, pp. 1437-1454, Feb. 2012.
- [15] P. Henry, M. Krainin, E. Herbst, X. Ren, and D. Fox, "RGB-D mapping: Using Kinect-style depth cameras for dense 3D modeling of indoor environments," *Int. J. Robot Res.*, vol. 31 no. 5, pp. 647-663, Ap. 2012.
- [16] S. Nissimov, J. Goldberger, and V. Alchanatis, "Obstacle detection in greenhouse environment using the Kinect sensor," *Comput. Electron. Agr.*, vol. 113, pp. 104-115, Ap. 2015.
- [17] T.J.M. Sanguino and F.P. Gomez, "Towards Simple Strategy for Optimal Tracking and Localization of Robots with Adaptive Particle Filtering," *IEEE-ASME T. Mech.*, (In Press)
- [18] C. Nock, O. Taugourdeau, S. Delagrèze, and C. Messier, "Assessing the potential of low-cost 3D cameras for the rapid measurement of plant woody structure," *Sensors* vol. 13, no.12, pp. 16216-16233, Nov. 2013.
- [19] S. Paulus, J. Behmann, A.-K. Mahlein, L. Plümer, and H. Kuhlmann, "Low-cost 3D systems: suitable tools for plant phenotyping," *Sensors* vol. 14, no.2, pp. 3001-3018, Feb. 2014.
- [20] D. Andújar, D. C. Fernández-Quintanilla, and J. Dorado, "Matching the best viewing angle in depth cameras for biomass estimation based on poplar seedling geometry," *Sensors* vol. 15, no.6, pp. 12999-13011, Jun. 2015.
- [21] Y. Chéné, D. Rousseau, P. Lucidarme, J. Bertheloot, V. Caffier, P. Morel, É. Belin, and F. Chapeau-Blondeau, "On the use of depth camera for 3D phenotyping of entire plants," *Comput. Electron. Agr.*, vol. 82, pp. 122-127, Mar. 2012.
- [22] T.T. Ngyuen, K. Vandevoorde, N. Wouters, E. Kayacan, J.G.D. Baerdemaeker, and W. Saeys, "Detection of red and bicoloured apples on tree with an RGB-D camera," *Biosyst. Eng.*, vol. 146, pp. 33-44, Jun. 2016.
- [23] F. Auat Cheein, G. Steiner, G. Perez Paina, and R. Carelli, "Optimized EIF-SLAM algorithm for precision agriculture mapping based on stems detection," *Comput. Electron. Agr.*, vol. 78, no. 2, pp. 195-207, Sep. 2011.
- [24] F. Endres, J. Hess, N. Engelhard, J. Sturm, D. Cremers, W. Burgard, "3-D Mapping with an RGB-D Camera," *IEEE T. Robot.*, vol. 30 no.1, pp. 177-187, Feb. 2014.



**Joan Ramon Rosell** received the M.Sc. degree in physics from the University of Barcelona, Spain, in 1986, the Ph.D. degree in physics (nuclear engineering) from the Polytechnical University of Catalonia (UPC), Barcelona, in 1989, and the Bachelor's Degree in electrical engineering from the Rovira i Virgili University, Tarragona, Spain, in 1997. From 1986 to 1992, he was assistant and associate professor at UPC. Since 1992, he has been with the Department of Agricultural and Forest Engineering, University of Lleida, where he is currently an Associate Professor and a Member of the Research Group in AgroICT & Precision Agriculture (GRAP). His research interests include precision agriculture, sensors, automation, and electrical engineering.



**Eduard Gregorio** received the M.Sc. degree in industrial engineering from the Polytechnical University of Catalonia (Catalonia, Spain), in 2005 and the Ph.D. from the University of Lleida, in 2012. Since 2009, he has been with the Department of Agricultural and Forest Engineering, University of Lleida, where he is currently an Assistant Professor and a Member of the Research Group in Precision Agriculture (GRAP). His research interests include the use of sensors in agriculture, LiDAR remote sensing, and electrical engineering.



**Jordi Gené** received the M.Sc. degree in industrial engineering from the University of Lleida (Catalonia, Spain), in 2015. He is currently working toward the Ph.D. degree in the Research Group in Precision Agriculture (GRAP), Department of Agricultural and Forest Engineering, University of Lleida. His research interests include remote sensing and electronic characterization of vegetation.



**Jordi Llorens** receives the Bachelor's Degree in agricultural engineering from Polytechnical University of Catalonia, Barcelona, Spain, in 2002. He received the Master's Degree in agricultural engineering from the University of Lleida, Lleida, Spain, in 2005, and the Ph.D. degree in Agri Food Engineering and

Biotechnology from Polytechnical University of Catalonia, Castelldefels, Spain, in 2012.

He worked at Cornell University at the Department of Entomology, Ithaca, US, in 2012-2013, as a postdoctoral associate in New York State Agricultural Experiment Station in Geneva. He worked at University of Córdoba at the Department of Rural Engineering, Córdoba, Spain, in 2014-2015 as a specialist engineer. Since January 2015, he has been working in the Research Group in AgroICT & Precision Agriculture, Department of Agricultural and Forest Engineering, University of Lleida as postdoctoral researcher. His research interests include precision agriculture, global positioning systems, programming of electronic devices, development of software for mobile devices and open source hardware and software.



**Xavier Torrent** received the Bachelor's Degree in Agricultural and Food Engineering from the University of Lleida (Catalonia, Spain) in 2009 and M.Sc. degree in Agricultural Engineering from the University of Lleida, in 2013. He is currently working toward the Ph.D. degree in Agricultural and Food Science

and Technology in the Research Group in AgroICT & Precision Agriculture (GRAP), Department of Agricultural and Forest Engineering, University of Lleida. His research interests include the use of sensors in agriculture, sustainable and precision application of pesticides (spray application technology, spray drift, droplet characterization, and operator exposure), LiDAR remote sensing, and fluid dynamics.



**Jaume Arnó**, MSc, Agricultural Engineer, obtains his Ph.D. in 2008 from the University of Lleida (Catalonia, Spain). He currently works as associate professor at the same university in the area of agricultural and forest engineering. Member of the Research Group in Precision Agriculture (GRAP), their research is focused on the

use of sensors in agriculture, spatial data analysis, and development of systems for decision support and field sampling.



**Alexandre Escolà** received the M.Sc. degree in Agricultural Engineering from the University of Lleida (Catalonia, Spain), in 2001 and the Ph.D. from the University of Lleida, in 2010. Since 2001, he has been at the Department of Agricultural and Forest Engineering of the University of Lleida, where he is currently an equivalent

of Associate Professor and a Member of the Research Group in AgroICT & Precision Agriculture (GRAP). His research interests include the use of sensors in agriculture, LiDAR remote sensing, and precision agriculture.